Journal of Stress Analysis
Vol. 4, No. 1, Spring − Summer 2019

Bu-Ali Sina University

Effect of Hygrothermal Environmental Conditions on the Time-dependent Creep Response of Functionally Graded Magneto-electro-elastic Hollow Sphere

M. Saadatfar*
Mechanical Engineering Department, University of Qom, Qom, Iran.

Article info

Article history:
Received 08 January 2019
Received in revised form
26 June 2019
Accepted 27 July 2019

Keywords:
FGMEE
Hygrothermal loading
Time-dependent creep
Hollow sphere

Abstract

In this paper, hygro-thermo-magneto-electro-elastic creep stress redistribution of a functionally graded magneto-electro-elastic (FGMEE) hollow sphere is examined. It is supposed that all material properties are a power-law function of radius. Temperature and moisture concentration functions are obtained analytically and then, a differential equation with creep strains is obtained using equations of electrostatic, magnetostatic and equilibrium, At first, ignoring the creep strains, a solution for the initial hygro-thermo-magneto-electroelastic stresses at zero time is achieved. Subsequently, creep strains are considered and creep stress rates are obtained. The Prandtl-Reuss equations and Norton's law are taken for the creep analysis. Finally, time-dependent creep stresses as well as magnetic and potential field redistributions at any time are obtained using an iterative method. Results show that the radial stress, radial displacement, electric potential and magnetic potentials increase as time goes by at a decreasing rate. Also, the grading index and hygrothermal condition have more considerable effect on the radial stress after creep evolution rather than initial case. Thus, their effects must be considered in creep evolution analysis.

Nomenclature

B_r	Magnetic induction	β_i	Moisture expansion coefficients
c_{ij}	Elastic coefficients	D_r	Electric displacement
d_{11}	Magnetic coefficient	e_{1j}	Piezoelectric coefficient
k^C	Moisture diffusivity coefficient	k^T	Thermal conductivity coefficient
m_1	Pyromagnetic coefficient	p_1	Pyroelectric coefficient
q_{1j}	Piezomagnetic coefficient	α_i	Thermal modulus coefficients
ψ	Magnetic potential	β_{11}	Dielectric coefficient
C_{ij0}	Temperature and moisture independent elastic coefficient	β^*	Empirical material coefficient for moisture dependence
γ_1	Hygromagnetic coefficient	ε_{11}	Electromagnetic coefficient
$\dot{\varepsilon}_i^c$	Creep strain rate	$\dot{\varepsilon}_e^c$	Effective creep strain rate
ζ_i	Hygroscopic stress coefficients	ρ	Density
σ_e	Effective stress	σ_i	Stresses
α^*	Empirical material coefficient for temperature dependence	χ_1	Hygroelectric coefficient
		ϕ	Electric potential

*Corresponding author: M. Saadatfar (Assistant Professor)
E-mail address: m.saadatfar@gmail.com
http://dx.doi.org/10.22084/jrstan.2019.18157.1080
ISSN: 2588-2597

1. Introduction

Magneto-electro-elastic (MEE) materials have simultaneous piezoelectric, piezomagnetic, and particularly magnetoelectric coupling effects. Owing to this multifunctional ability in sensing and actuating, they have found to have several applications in the area of aerospace structures, damage detection, structural health monitoring and energy harvesting [1]. In addition, due to the benefits of functionally graded materials (FGMs) [2, 3], FGMEE was suggested. It is feasible to increase displacements and decrease stresses in functionally graded actuators [4-6]. Given that these materials are usually used under various loadings and different environments, the analysis of the effects of moisture and temperature on their performances is of vital importance. Also, under severe conditions, these materials show obvious creep property in time as a result of their inherent viscoelastic property [7]. Consequently, the investigation of the time-dependent behavior of these structures under multiphysical conditions is vital.

For MEE spherical structure, the dynamic response of MEE hollow sphere was investigated by Wang and Ding [8, 9]. Transient thermal stress in a multilayered MEE hollow sphere was investigated by Ootao and Ishihara [10]. Chen et al. [11] presented a solution for the spherically anisotropic MEE hollow sphere problem. Saadatfar and Aghaie-Khafri [12] considered the response of a FGMEE sphere in a hygrothermal condition.

In the area of multiphysical analysis, several problems have been considered by researchers to discover the multiphysical behavior of intelligent structures. The coupled hygrothermal stress of laminated plates was studied by Smittakorn and Heyliger [13]. Besides, they [14] disclosed the effects of the hygro-thermo-electro-mechanical conditions on the response of composite plates. Using the finite element method, Raja et al. [15] studied the hygro-thermo-piezoelectric interactions in laminated plates and shells. Saadatfar and Aghaie-Khafri [16, 17] disclosed that the actuation and sensing authority of FGPM layers was widely affected by their inhomogeneity index under hygro-thermo-electro-mechanical loading. Later, Saadatfar [18] presented hygro-thermo-magneto-electro-elastic analysis of a finite hybrid FGM cylindrical shell with FGPM layers using differential quadrature method (DQM).

Some articles are available on creep behaviors in FGM and piezoelectric spheres. You and Ou [19] carried out creep investigation of hollow sphere with variable creep properties. Loghman and Shokouhi [20] investigated creep stresses in a hollow sphere using a long-term creep model. Loghman et al. [21, 22] conducted a time-dependent creep analysis of FGM spheres. Dai et al. [7] presented the creep analysis of a FGPM sphere subjected to thermo-electro-mechanical loads. Jafari Fesharaki et al. [23] investigated the time-dependent response of a FGM thick-walled sphere under thermomechanical loads using the method of successive elastic solution. Ghorbanpour Arani et al. [24] obtained the history of stresses in a thick-walled piezoelectric sphere under thermo-mechanical loads employing Mendelson's method. Jabbari and Tayebi [25] derived an analytical solution for creep stresses of a thick-walled sphere made of porous FGPM in a magnetic field. Using Burgers' creep model, Loghman and Tourang [26] investigated non-stationary creep response of a smart sphere made of polyvinylidene fluoride (PVDF). To the best of the authors' knowledge, time-dependent creep analysis of a FGMEE thick-walled sphere with hygrothermal gradient has not yet been conducted. Therefore, using the Prandtl-Reuss equations and Norton's law, this paper studied the creep stress redistribution for FGMEE hollow sphere for the first time, to discover the effects of potential interactions of various fields on the structural response of FGMEE hollow spheres.

2. Formulation of the Problem

A FGMEE thick-walled sphere which is radially polarized and magnetized is considered as shown in Fig. 1. The inner and outer radius are considered as a and b, respectively. Regarding spherically symmetric, magnetic and electric potentials, displacement, temperature and moisture concentration are the functions of radius. All material coefficients are assumed to be a simple power-law function of radius as: $\xi(r) = \bar{\xi} r^{\beta}$, $\xi = c_{ij}$, e_{1j}, q_{1j}, β_{11}, ε_{11}, d_{11}, p_1, m_1, α_i, k^T, k^C, χ_1, γ_1, β_i. Where, $\bar{\xi}$ indicate corresponding material coefficients and β is the grading parameter. c_{ij}, e_{1j}, q_{1j}, β_{11}, ε_{11}, d_{11}, p_1, m_1, α_i, k^T, k^C, χ_1, γ_1 and β_i are the elastic, piezoelectric, piezomagnetic, dielectric, electromagnetic, magnetic, pyroelectric, pyromagnetic, thermal expansion, thermal conductivity, moisture diffusivity, hygroelectric, hygromagnetic and moisture expansion coefficients, respectively.

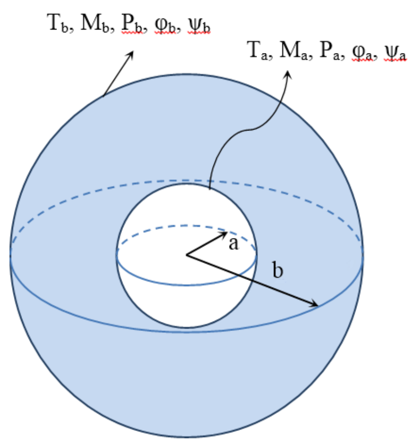

Fig. 1. FGMEE sphere.

2.1. Temperature and Moisture Concentration Problem

In an uncoupled hygrothermal analysis, the temperature and moisture concentration functions are obtained independently by solving heat conduction and moisture diffusion equations. The heat conduction and moisture diffusion equations in axisymmetric and steady-state condition are presented as [27]:

$$\frac{1}{r^2}\frac{\partial}{\partial r}\left(r^2 k^T \frac{\partial T}{\partial r}\right) = 0, \tag{1a}$$

$$\frac{1}{r^2}\frac{\partial}{\partial r}\left(r^2 k^C \frac{\partial M}{\partial r}\right) = 0, \tag{1b}$$

Integrating these equations twice yields:

$$\begin{aligned} T(r) &= W_1 r^{-\beta-1} + W_2, \\ M(r) &= S_1 r^{-\beta-1} + S_2\cdot \end{aligned} \tag{2}$$

The general hygrothermal boundary conditions can be written as:

$$\begin{aligned} C_{11}T'(a) + C_{12}T(a) &= f_1, \\ C_{21}T'(b) + C_{22}T(b) &= f_2, \end{aligned} \tag{3}$$

where C_{ij} is the Robin-type boundary condition coefficients and f_1 and f_2 are known constants on the inner and outer radius. Using these boundary conditions and the constants W_i, one can write [28]:

$$\begin{aligned} W_1 =& \frac{C_{22}f_1 - C_{12}f_2}{C_{12}((\beta+1)C_{21}b^{-(\beta+2)} - C_{22}b^{-(\beta+1)}) - C_{22}((\beta+1)C_{11}\bar{a}^{(\beta+2)} - C_{12}a^{-(\beta+1)})} \\ W_2 =& \frac{f_1((\beta+1)C_{21}b^{-(\beta+2)} - C_{22}b^{-(\beta+1)}) - f_2((\beta+1)C_{11}\bar{a}^{(\beta+2)} - C_{12}a^{-(\beta+1)})}{C_{12}((\beta+1)C_{21}b^{-(\beta+2)} - C_{22}b^{-(\beta+1)}) - C_{22}((\beta+1)C_{11}\bar{a}^{(\beta+2)} - C_{12}a^{-(\beta+1)})} \end{aligned} \tag{4}$$

The constants S_i can be obtained in the same way for general hygrothermal boundary conditions. In this study, the moisture concentration and temperature inside and outside of the sphere are taken to be M_a, M_b, T_a and T_b, respectively. Thus, the constants can be obtained as:

$$\begin{aligned} W_1 &= \frac{T_a - T_b}{a^{-(\beta+1)} - b^{-(\beta+1)}}, \\ W_2 &= \frac{-T_a b^{-(\beta+1)} + T_b a^{-(\beta+1)}}{a^{-(\beta+1)} - b^{-(\beta+1)}} \end{aligned} \tag{5a}$$

$$\begin{aligned} S_1 &= \frac{M_a - M_b}{a^{-(\beta+1)} - b^{-(\beta+1)}}, \\ S_2 &= \frac{-M_a b^{-(\beta+1)} + M_b a^{-(\beta+1)}}{a^{-(\beta+1)} - b^{-(\beta+1)}} \end{aligned} \tag{5b}$$

2.2. Basic Equations of the Problem

It is assumed that total strains are the sum of hygrothermal, electric, magnetic, elastic and creep strains. Therefore, the stress-strain relation can be expressed as:

$$\begin{aligned} \sigma_r = c_{11}\frac{\partial u}{\partial r} + 2c_{12}\frac{u}{r} + e_{11}\frac{\partial \phi}{\partial r} + q_{11}\frac{\partial \psi}{\partial r} - \lambda_1 T \\ - \zeta_1 M - c_{11}\varepsilon_{rr}^c - 2c_{12}\varepsilon_{\theta\theta}^c \end{aligned} \tag{6a}$$

$$\begin{aligned} \sigma_\theta = c_{12}\frac{\partial u}{\partial r} + (c_{22}+c_{23})\frac{u}{r} + e_{12}\frac{\partial \phi}{\partial r} + q_{12}\frac{\partial \psi}{\partial r} - \lambda_2 T \\ - \zeta_2 M - c_{12}\varepsilon_{rr}^c - (c_{22}+c_{23})\varepsilon_{\theta\theta}^c, \end{aligned} \tag{6b}$$

$$\begin{aligned} D_r = e_{11}\frac{\partial u}{\partial r} + 2e_{12}\frac{u}{r} - \beta_{11}\frac{\partial \phi}{\partial r} - \varepsilon_{11}\frac{\partial \psi}{\partial r} + p_1 T + \chi_1 M \\ - e_{11}\varepsilon_{rr}^c - 2e_{12}\varepsilon_{\theta\theta}^c, \end{aligned} \tag{6c}$$

$$\begin{aligned} B_r = q_{11}\frac{\partial u}{\partial r} + 2q_{12}\frac{u}{r} - \varepsilon_{11}\frac{\partial \phi}{\partial r} - d_{11}\frac{\partial \psi}{\partial r} + m_1 T + \gamma_1 M \\ - q_{11}\varepsilon_{rr}^c - 2q_{12}\varepsilon_{\theta\theta}^c \end{aligned} \tag{6d}$$

where $\sigma_i(r)$ $(i = r, \theta)$, ϕ, ψ, D_r and B_r are components of stress, electric and magnetic potentials, electric displacement and magnetic induction, respectively. Also, we have:

$$\begin{aligned} \lambda_1 &= c_{11}\alpha_r + 2c_{12}\alpha_\theta, \\ \lambda_2 &= c_{12}\alpha_r + (c_{22}+c_{23})\alpha_\theta, \end{aligned} \tag{7a}$$

$$\begin{aligned} \zeta_1 &= c_{11}\beta_r + 2c_{12}\beta_\theta, \\ \zeta_2 &= c_{12}\beta_r + (c_{22}+c_{23})\beta_\theta, \end{aligned} \tag{7b}$$

Without body forces, the equation of equilibrium is:

$$\frac{\partial \sigma_r}{\partial r} + \frac{2(\sigma_r - \sigma_\theta)}{r} = 0\cdot \tag{8}$$

The electrostatic and magnetostatic equations, without electric charge and electric current densities, are:

$$\frac{\partial D_r}{\partial r} + \frac{2D_r}{r} = 0, \tag{9a}$$

$$\frac{\partial B_r}{\partial r} + \frac{2B_r}{r} = 0\cdot \tag{9b}$$

The boundary conditions are assumed as follow:

$$\sigma_r\Big|_{r=a} = -p_a, \quad \sigma_r\Big|_{r=b} = -p_b,$$
$$\phi\Big|_{r=a} = \phi_a, \quad \phi\Big|_{r=b} = \phi_b, \tag{10}$$
$$\psi\Big|_{r=a} = \psi_a, \quad \psi\Big|_{r=b} = \psi_b.$$

Solving Eqs. (9), yields:

$$D_r = \frac{A_1}{r^2}, \tag{11a}$$

$$B_r = \frac{A_2}{r^2}, \tag{11b}$$

Where, A_1 and A_2 are unknown constants. Substituting Eqs. (11) into Eqs. (6c) and (6d), yields:

$$\frac{\partial\phi(r)}{\partial r} = \frac{1}{\beta_{11}}\left(e_{11}\frac{\partial u}{\partial r} + 2e_{12}\frac{u}{r} - \varepsilon_{11}\frac{\partial\psi}{\partial r} - \frac{A_1}{r^2} + p_1 T + \chi_1 M - e_{11}\varepsilon^c_{rr} - 2e_{12}\varepsilon^c_{\theta\theta}\right) \tag{12a}$$

$$\frac{\partial\psi(r)}{\partial r} = \frac{1}{d_{11}}\left(q_{11}\frac{\partial u}{\partial r} + 2q_{12}\frac{u}{r} - \varepsilon_{11}\frac{\partial\phi}{\partial r} - \frac{A_2}{r^2} + m_1 T + \gamma_1 M - q_{11}\varepsilon^c_{rr} - 2q_{12}\varepsilon^c_{\theta\theta}\right) \tag{12b}$$

These equations can be rearranged as:

$$\frac{\partial\phi(r)}{\partial r} = \left(L_1\frac{\partial u}{\partial r} + 2L_2\frac{u}{r} + L_3\frac{A_2}{r^{2+\beta}} + L_4 T + L_6 M - L_5\frac{A_1}{r^{2+\beta}} - L_1\varepsilon^c_{rr} - 2L_2\varepsilon^c_{\theta\theta}\right) \tag{13a}$$

$$\frac{\partial\psi(r)}{\partial r} = \left(P_1\frac{\partial u}{\partial r} + 2P_2\frac{u}{r} + P_3\frac{A_1}{r^{2+\beta}} + P_4 T + P_6 M - P_5\frac{A_2}{r^{2+\beta}} - P_1\varepsilon^c_{rr} - 2P_2\varepsilon^c_{\theta\theta}\right) \tag{13b}$$

where,

$$L_1 = \frac{\bar{e}_{11}\bar{d}_{11} - \bar{\varepsilon}_{11}\bar{q}_{11}}{\bar{\beta}_{11}\bar{d}_{11} - \bar{\varepsilon}^2_{11}}, \quad L_2 = \frac{\bar{e}_{12}\bar{d}_{11} - \bar{\varepsilon}_{11}\bar{q}_{12}}{\bar{\beta}_{11}\bar{d}_{11} - \bar{\varepsilon}^2_{11}}$$
$$L_3 = \frac{\bar{\varepsilon}_{11}}{\bar{\beta}_{11}\bar{d}_{11} - \bar{\varepsilon}^2_{11}}, \quad L_4 = \frac{\bar{d}_{11}\bar{p}_1 - \bar{\varepsilon}_{11}\bar{m}_1}{\bar{\beta}_{11}\bar{d}_{11} - \bar{\varepsilon}^2_{11}}$$
$$L_5 = \frac{\bar{d}_{11}}{\bar{\beta}_{11}\bar{d}_{11} - \bar{\varepsilon}^2_{11}}, \quad L_6 = \frac{\bar{d}_{11}\bar{\chi}_1 - \bar{\varepsilon}_{11}\bar{\gamma}_1}{\bar{\beta}_{11}\bar{d}_{11} - \bar{\varepsilon}^2_{11}}$$

$$P_1 = \frac{\bar{q}_{11}\bar{\beta}_{11} - \bar{\varepsilon}_{11}\bar{e}_{11}}{\bar{\beta}_{11}\bar{d}_{11} - \bar{\varepsilon}^2_{11}}, \quad P_2 = \frac{\bar{q}_{12}\bar{\beta}_{11} - \bar{e}_{12}\bar{\varepsilon}_{11}}{\bar{\beta}_{11}\bar{d}_{11} - \bar{\varepsilon}^2_{11}}$$
$$P_3 = \frac{\bar{\varepsilon}_{11}}{\bar{\beta}_{11}\bar{d}_{11} - \bar{\varepsilon}^2_{11}}, \quad P_4 = \frac{\bar{\beta}_{11}\bar{m}_1 - \bar{\varepsilon}_{11}\bar{p}_1}{\bar{\beta}_{11}\bar{d}_{11} - \bar{\varepsilon}^2_{11}} \tag{14}$$
$$P_5 = \frac{\bar{\beta}_{11}}{\bar{\beta}_{11}\bar{d}_{11} - \bar{\varepsilon}^2_{11}}, \quad P_6 = \frac{\bar{\beta}_{11}\bar{\gamma}_1 - \bar{\varepsilon}_{11}\bar{\chi}_1}{\bar{\beta}_{11}\bar{d}_{11} - \bar{\varepsilon}^2_{11}}$$

Substituting Eq. (13) into Eqs. (6a) and (6b) gives:

$$\sigma_r = C_1 r^\beta\frac{\partial u}{\partial r} + 2C_2 r^\beta\frac{u}{r} + C_3\frac{A_2}{r^2} + C_4\frac{A_1}{r^2} + C_5 r^\beta T + C_6 r^\beta M - \bar{\lambda}_1 r^{2\beta}T - \bar{\zeta}_1 r^{2\beta}M - C_1 r^\beta\varepsilon^c_{rr} - 2C_2 r^\beta\varepsilon^c_{\theta\theta}, \tag{15a}$$

$$\sigma_\theta = E_1 r^\beta\frac{\partial u}{\partial r} + 2E_2 r^\beta\frac{u}{r} + E_3\frac{A_2}{r^2} + E_4\frac{A_1}{r^2} + E_5 r^\beta T + E_6 r^\beta M - \bar{\lambda}_2 r^{2\beta}T - \bar{\zeta}_2 r^{2\beta}M - E_1 r^\beta\varepsilon^c_{rr} - 2E_2 r^\beta\varepsilon^c_{\theta\theta}, \tag{15b}$$

where,

$$\begin{aligned}
C_1 &= \bar{c}_{11} + \bar{e}_{11}L_1 + \bar{q}_{11}P_1,\\
C_2 &= \bar{c}_{12} + \bar{e}_{11}L_2 + \bar{q}_{11}P_2,\\
C_3 &= \bar{e}_{11}L_3 - \bar{q}_{11}P_5,\\
C_4 &= -\bar{e}_{11}L_5 + \bar{q}_{11}P_3,\\
C_5 &= -\bar{e}_{11}L_4 + \bar{q}_{11}P_4,\\
C_6 &= \bar{e}_{11}L_6 + \bar{q}_{11}P_6,\\
E_1 &= \bar{c}_{12} + \bar{e}_{12}L_1 + \bar{q}_{12}P_1,\\
E_2 &= \left(\frac{\bar{c}_{22} + \bar{c}_{23}}{2}\right) + \bar{e}_{12}L_2 + \bar{q}_{12}P_2,\\
E_3 &= \bar{e}_{12}L_3 - \bar{q}_{12}P_5,\\
E_4 &= -\bar{e}_{12}L_5 + \bar{q}_{12}P_3,\\
E_5 &= \bar{e}_{12}L_4 + \bar{q}_{12}P_4,\\
E_6 &= \bar{e}_{12}L_6 + \bar{q}_{12}P_6
\end{aligned} \tag{16}$$

Substituting Eqs. (15) into Eq. (8), the equilibrium equation is now can be expressed as:

$$\frac{\partial^2 u}{\partial r^2} + \frac{1}{r}M_1\frac{\partial u}{\partial r} + \frac{1}{r^2}M_2 u = M_3 r^{\beta-1}T + M_4\frac{T}{r} + (-M_5 + M_6 r^\beta)\frac{\partial T}{\partial r} + M_7\frac{A_2}{r^{3+\beta}} + M_8\frac{A_1}{r^{3+\beta}} + M_9 r^{\beta-1}M + M_{10}\frac{M}{r} + (-M_{11} + M_{12}r^\beta)\frac{\partial M}{\partial r} + M_{13}r^{-1}\varepsilon^c_{rr} + \frac{\partial\varepsilon^c_{rr}}{\partial r} + 2M_{14}r^{-1}\varepsilon^c_{\theta\theta} + 2M_{15}\frac{\partial\varepsilon^c_{\theta\theta}}{\partial r} \tag{17}$$

where,

$$\begin{aligned}
M_1 &= \frac{C_1(\beta+2)+2C_2-2E_1}{C_1},\\
M_2 &= \frac{2C_2(\beta+1)-4E_2}{C_1},\\
M_3 &= \frac{2(\bar{\lambda}_1(\beta-2)+\bar{\lambda}_2)}{C_1},\\
M_4 &= \frac{2E_5-C_5(\beta+2)}{C_1},\\
M_5 &= \frac{C_5}{C_1},\\
M_6 &= \frac{\bar{\lambda}_1}{C_1},\\
M_7 &= \frac{2E_3}{C_1},\\
M_8 &= \frac{2E_4}{C_1},\\
M_9 &= \frac{2(\bar{\zeta}_1(\beta-2)+\bar{\zeta}_2)}{C_1},\\
M_{10} &= \frac{2E_6-C_6(\beta+2)}{C_1},\\
M_{11} &= \frac{C_6}{C_1},\\
M_{12} &= \frac{\bar{\zeta}}{C_1},\\
M_{13} &= \frac{C_1(\beta+2)-2E_1}{C_1},\\
M_{14} &= \frac{C_2(\beta+2)-2E_2}{C_1},\\
M_{15} &= \frac{C_2}{C_1}
\end{aligned} \tag{18}$$

3. Solution of the Equations

3.1. Initial Stress Analysis

To determine initial stresses, ignoring creep strains in Eq. (17), the following differential equation was obtained using Eqs. (2) in to Eq. (17):

$$\begin{aligned}
&\frac{\partial^2 u}{\partial r^2}+\frac{M_1}{r}\frac{\partial u}{\partial r}+\frac{M_2}{r^2}u=(M_3W_2+M_9S_2)r^{\beta-1}\\
&+(M_4W_2+M_{10}S_2)r^{-1}+\big[W_1(M_4+M_5(\beta+1))\\
&+S_1(M_{10}+M_{11}(\beta+1))\big]r^{-\beta-2}+\big[W_1(M_3-M_6(\beta+1)\\
&+S_1(M_9-M_{12}(\beta+1))\big]r^{-2}+M_7\frac{A_2}{r^{3+\beta}}+M_8\frac{A_1}{r^{3+\beta}}\cdot
\end{aligned} \tag{19}$$

The solution of Eq. (19) may be considered as:

$$u=u_g+u_p\cdot \tag{20}$$

The homogeneous solution of the Eq. (20) can be found as:

$$u_g=B_1r^{m_1}+B_2r^{m_2}, \tag{21}$$

where B_1 and B_2 are constants and we have:

$$m_{1,2}=\frac{1}{2}\big(-(M_1-1)\pm\sqrt{(M_1-1)^2-4M_2}\big)\cdot \tag{22}$$

In order to use numerical values, real, distinct roots will only be considered for every value of β [12]. Therefore, the stress expressions will be written using Eq. (22). Here, different magnitudes of β are used to discover its effect on the response of FGMEE thick-walled sphere. However, these magnitudes of are not necessarily related to a specific material. The particular solution of Eq. (19) can be considered as:

$$\begin{aligned}
u_p&=B_3r+B_4r^{\beta+1}+B_5r^{-\beta}+B_6\\
&+B_7A_2r^{-(\beta+1)}+B_8A_1r^{-(\beta+1)},
\end{aligned} \tag{23}$$

where,

$$\begin{aligned}
B_3&=\frac{M_4W_2+M_{10}S_2}{M_1+M_2},\\
B_4&=\frac{M_3W_2+M_9S_2}{M_2+(\beta+1)(\beta+M_1)}\\
B_5&=\frac{W_1\big(M_4+M_5(\beta+1)+S_1(M_{10}+M_{11}(\beta+1)\big)}{\beta(\beta+1)-\beta M_1+M_2}\\
B_6&=\frac{W_1(M_3-M_6(\beta+1)+S_1(M_9-M_{12}(\beta+1))}{M_2},\\
B_7&=\frac{M_7}{(\beta+1)(\beta+2-M_1)+M_2},\\
B_8&=\frac{M_8}{(\beta+1)(\beta+2-M_1)+M_2}\cdot
\end{aligned} \tag{24}$$

Thus, the complete solution is:

$$\begin{aligned}
u&=u+u_p\\
&=B_1r^{m_1}+B_2r^{m_2}+B_3r+B_4r^{\beta+1}+B_5r^{-\beta}\\
&+B_6+B_7A_2r^{-(\beta+1)}+B_8A_1r^{-(\beta+1)}.
\end{aligned} \tag{25}$$

When u(r) is known, Eq. (13a) can be expressed as:

$$\begin{aligned}
&\frac{\partial\phi(r)}{\partial r}=\Big(L_1\big(B_1m_1r^{m_1-1}+B_2m_2r^{m_2-1}+B_3\\
&+B_4(\beta+1)r^{\beta}-B_5\beta r^{-(\beta+1)}-(\beta+1)B_8A_1r^{-(\beta+2)}\\
&-(\beta+1)B_7A_2r^{(\beta+2)}\big)\Big)+2L_2\Big(\beta_1r^{m_1-1}+B_2r^{m_2-1}+B_3\\
&+B_4r^{\beta}+B_5r^{-(\beta+1)}+B_8A_1r^{-(\beta+2)}+B_7A_2r^{-(\beta+2)}+\frac{B_6}{r}\Big)\\
&+L_3\frac{A_2}{r^{2+\beta}}-L_5\frac{A_1}{r^{2+\beta}}+L_4\big(W_1r^{-(\beta+1)}+W_2\big)\\
&+L_6\big(S_1r^{-(\beta+1)}+S_2\big)\cdot
\end{aligned} \tag{26}$$

Integrating Eq. (26), we have:

$$\phi(r) = \Big(L_1\big(B_1 r^{m_1} + B_2 r^{m_2} + B_3 r + B_4 r^{\beta+1} + B_5 r^{-\beta} - B_8 A_1 r^{-(\beta+1)} + B_7 A_2 r^{-(\beta+1)}\big)\Big) + 2L_2\left(\frac{B_1}{m_1} r^{m_1} + \frac{B_2}{m_2} r^{m_2} + B_3 r + \frac{B_4}{\beta+1} r^{\beta+1} - \frac{B_5}{\beta} r^{-\beta} - \frac{B_8 A_1}{(\beta+1)} r^{-(\beta+1)} - \frac{B_7 A_2}{(\beta+1)} r^{-(\beta+1)} + B_6 \ln(r)\right) - L_3 \frac{A_2}{(\beta+1)} r^{-(\beta+1)} + L_5 \frac{A_1}{(\beta+1)} r^{-(\beta+1)} + L_4\left(-\frac{W_1}{\beta} r^{-\beta} + W_2 r\right) + L_6\left(-\frac{S_1}{\beta} r^{-\beta} + S_2 r\right) + Z_1\cdot \quad (27)$$

Where Z_1 is a constant. Likewise, $\psi(r)$ can be written as:

$$\psi(r) = \Big(P_1\big(B_1 r^{m_1} B_2 r^{m_2} + B_3 r + B_4 r^{\beta+1} + B_5 r^{-\beta} + B_8 A_1 r^{-(\beta+1)} + B_7 A_1 r^{-(\beta+1)}\big)\Big) + 2P_2\left(\frac{B_1}{m_1} r^{m_1} + \frac{B_2}{m_2} r^{m_2} + B_3 r + \frac{B_4}{\beta+1} r^{\beta+1} - \frac{B_5}{\beta} r^{-\beta} - \frac{B_8 A_1}{(\beta+1)} r^{-(\beta+1)} - \frac{B_7 A_2}{(\beta+1)} r^{-(\beta+1)} + B_6 \ln(r)\right) + P_5 \frac{A_2}{(\beta+1)} r^{-(\beta+1)} - P_3 \frac{A_1}{(\beta+1)} r^{-(\beta+1)} + P_4\left(-\frac{W_1}{\beta} r^{-\beta} + W_2 r\right) + P_6\left(-\frac{S_1}{\beta} r^{-\beta} + S_2 r\right) + Z_2\cdot \quad (28)$$

Where Z_2 is an unknown constant. Substituting Eq. (2), Eq. (23), Eq. (27) and (28) into Eq. (15), the initial radial and hoop stresses of the thick-walled FG-MEE sphere were obtained as:

$$\sigma_r = C_1 r^{\beta}\big(B_1 m_1 r^{m_1-1} + B_2 m_2 r^{m^2-1} + B_3 + B_4(\beta+1) r^{\beta} - B_5 \beta r^{-\beta-1} - (\beta+1) B_8 A_1 r^{-\beta-2} - (\beta+1) B_7 A_2 r^{-\beta-2}\big) + 2C_2 r^{\beta}\left(B_1 r^{m_1-1} + B_2 r^{m_2-1} + B_3 + B_4 r^{\beta} + B_5 r^{-(\beta+1)} + B_8 A_1 r^{-(\beta+2)} + B_7 A_2 r^{-(\beta+2)} + B_7 A_2 r^{-(\beta+2)} + \frac{B_6}{r}\right) + C_3 \frac{A_2}{r^2} + C_4 \frac{A_1}{r^2} + (C_5 r^{\beta} - \bar{\lambda}_1 r^{2\beta})(W_1 r^{-(\beta+1)} + W_2) + (C_6 r^{\beta} - \bar{\zeta}_1 r^{2\beta})(S_1 r^{-(\beta+1)} + S_2)\cdot \quad (29)$$

$$\sigma_\theta = E_1 r^{\beta}\big(B_1 m_1 r^{m_1-1} + B_2 m_2 r^{m_2-1} + B_3 + B_4(\beta+1) r^{\beta} - B_5 \beta r^{-\beta-1} - (\beta+1) B_8 A_1 r^{-\beta-2} - (\beta+1) B_7 A_2 r^{-\beta-2}\big) + 2E_2 r^{\beta}\left(B_1 r^{m_1-1} + B_2 r^{m_2-1} + B_3 + B_4 r^{\beta} + B_5 r^{-(\beta+1)} + B_8 A_1 r^{-(\beta+2)} + B_7 A_2 r^{-(\beta+2)} + \frac{B_6}{r}\right) + E_3 \frac{A_2}{r^2} + E_4 \frac{A_1}{r^2} + (E_5 r^{\beta} - \bar{\lambda}_2 r^{2\beta})(W_1 r^{-(\beta+1)} + W_2) + (E_6 r^{\beta} - \bar{\zeta}_2 r^{2\beta})(S_1 r^{-(\beta+1)} + S_2)\cdot \quad (30)$$

Employing the electro-magneto-mechanical boundary conditions, the unknown constants A_1, A_2, B_1, B_2, Z_1 and Z_2 can be found by solving the system of six linear algebraic equations which can be expressed as:

$$X[B_1 \;\; B_2 \;\; A_1 \;\; A_2 \;\; Z_1 \;\; Z_2]^T = F, \quad (31)$$

Where X and F are known matrix. Now, the initial stresses, radial displacement, electric and magnetic potential are known at zero time.

3.2. Time-dependent Creep Analysis

Assuming the temperature and moisture concentration to be constant-time, differentiation Eq. (17) with respect to time gives:

$$\frac{\partial^2 \dot{u}}{\partial r^2} + \frac{1}{r} M_1 \frac{\partial \dot{u}}{\partial r} + \frac{1}{r^2} M_2 \dot{u} = M_7 \frac{\dot{A}_2}{r^{3+\beta}} + M_8 \frac{\dot{A}_1}{r^{3+\beta}} + M_{13} r^{-1} \dot{\varepsilon}^c_{rr} + \frac{\partial \dot{\varepsilon}^c_{rr}}{\partial r} + 2M_{14} r^{-1} \dot{\varepsilon}^c_{\theta\theta} + 2M_{15} \frac{\partial \dot{\varepsilon}^c_{\theta\theta}}{\partial r} \quad (32)$$

Creep rates can be related to the stresses by the Prandtl-Reuss equations as [25, 29]:

$$\begin{aligned} \dot{\varepsilon}^c_r &= \frac{\dot{\varepsilon}^c_e}{\sigma_e}(\sigma_r - 0.5(\sigma_\theta + \sigma_\phi)) \\ \dot{\varepsilon}^c_\theta &= \frac{\dot{\varepsilon}^c_e}{\sigma_e}(\sigma_\theta - 0.5(\sigma_r + \sigma_\phi)) \\ \dot{\varepsilon}^c_\phi &= \frac{\dot{\varepsilon}^c_e}{\sigma_e}(\sigma_\phi - 0.5(\sigma_\theta + \sigma_r)) \end{aligned} \quad (33)$$

Where, $\dot{\varepsilon}^c_i$ $(i = r, \theta, \phi)$ is the creep strain rate, $\dot{\varepsilon}^c_e$ is the effective creep strain rate and σ_e is the effective stress. The Norton's law is considered as the creep constitutive model in the following form [25, 30]:

$$\dot{\varepsilon}^c_e = B(r) \sigma_e^{n(r)} \quad (34)$$

Where $B(r)$ and $n(r)$ are material creep parameters. They are considered as function of radius as [21, 31]:

$$B(r) = b_0 r^{b_1}, n(r) = n_0 \quad (35)$$

Where b_0, b_1 and n_0 are constants. Considering symmetry of the problem and substituting Eq. (35) into Eq. (33), gives:

$$\dot{\varepsilon}_r^c = B(r)\sigma_e^{n_0-1}(\sigma_\theta - \sigma_r) \qquad \dot{\varepsilon}_\theta^c = \frac{B(r)}{2}\sigma_e^{n_0-1}(\sigma_\theta - \sigma_r) \tag{36}$$

The Von Mises equivalent stress is considered as:

$$\sigma_e = \frac{1}{\sqrt{2}}\sqrt{(\sigma_\theta-\sigma_r)^2+(\sigma_\theta-\sigma_\phi)^2+(\sigma_\phi-\sigma_r)^2} = |\sigma_\theta - \sigma_r| \tag{37}$$

Using Eq. (37), Eq. (36) yields:

$$\dot{\varepsilon}_r^c = -B(r)\sigma_e^{n_0} \qquad \dot{\varepsilon}_\theta^c = \frac{B(r)}{2}\sigma_e^{n_0} \tag{38}$$

Substituting Eq. (38) into Eq. (32), gives:

$$\frac{\partial^2\dot{u}}{\partial r^2} + \frac{1}{r}M_1\frac{\partial \dot{u}}{\partial r} + \frac{1}{r^2}M_2\dot{u} = M_7\frac{\dot{A}_2}{r^{3+\beta}} + M_8\frac{\dot{A}_2}{r^{3+\beta}} + b_0r^{b_1-1}\sigma_e^{n_0}\big(M_{14}+M_{15}b_1 - M_{13} - b_1\big) + (M_{15}-1)b_0r^{b_1}\frac{\partial\sigma_e^{n_0}}{\partial r} \tag{39}$$

Using a similar method as in previous section, the solution can be expressed as:

$$\dot{u} = D_1r^{m_1} + D_2r^{m_2} + G_{11}r^{m_1} + G_{21}r^{m_2} + B_8r^{-(\beta+1)}\dot{A}_1 + B_7r^{-(\beta+1)}\dot{A}_2 \tag{40}$$

Where $G_{11}(r)$ and $G_{21}(r)$ can be achieved by method of variation of parameters as:

$$G_{11}(r) = \frac{b_0}{m_2-m_1}\int\left\{r^{b_1-m_1}\sigma_e^{n_0}(M_{14}+M_{15}b_1-M_{13}-b_1) + (M_{15}-1)r^{b_1-m_1+1}\frac{\partial\sigma_e^{n_0}}{\partial r}\right\}dr$$
$$G_{21}(r) = -\frac{b_0}{m_2-m_1}\int\left\{r^{b_1-m_2}\sigma_e^{n_0}(M_{14}+M_{15}b_1-M_{13}-b_1) + (M_{15}-1)r^{b_1-m_2+1}\frac{\partial\sigma_e^{n_0}}{\partial r}\right\}dr \tag{41}$$

Differentiation Eq. (15) and Eq. (13) with respect to time yields:

$$\dot{\sigma}_r = C_1r^\beta\frac{\partial\dot{u}}{\partial r} + 2C_2r^\beta\frac{\dot{u}}{r} + C_3\frac{\dot{A}_2}{r^2} + C_4\frac{\dot{A}_1}{r^2} + (C_1-C_2)b_0r^{b_1+\beta}\sigma_e^{n_0}, \tag{42a}$$

$$\dot{\sigma}_\theta = E_1r^\beta\frac{\partial\dot{u}}{\partial r} + 2E_2r^\beta\frac{\dot{u}}{r} + E_3\frac{\dot{A}_2}{r^2} + E_4\frac{\dot{A}_1}{r^2} + (E_1-E_2)b_0r^{b_1+\beta}\sigma_e^{n_0}, \tag{42b}$$

$$\frac{\partial\dot{\phi}}{\partial r} = L_1\frac{\partial\dot{u}}{\partial r} + 2L_2\frac{\dot{u}}{r} - L_5\frac{\dot{A}_1}{r^{2+\beta}} + L_3\frac{\dot{A}_2}{r^{2+\beta}} - L_1\dot{\varepsilon}_{rr}^c - 2L_2\dot{\varepsilon}_{\theta\theta}^c, \tag{42c}$$

$$\frac{\partial\dot{\psi}}{\partial r} = P_1\frac{\partial\dot{u}}{\partial r} + 2P_2\frac{\dot{u}}{r} + P_3\frac{\dot{A}_1}{r^{2+\beta}} - P_5\frac{\dot{A}_2}{r^{2+\beta}} - P_1\dot{\varepsilon}_{rr}^c - 2P_2\dot{\varepsilon}_{\theta\theta}^c \tag{42d}$$

Substituting Eq. (40) in Eq. (42) gives:

$$\dot{\sigma}_r = D_1((m_1C_1+2C_2)r^{\beta+m_1-1}) + D_2((m_2C_1+2C_2)r^{\beta+m_2-1}) + (B_8(2C_2-C_1(1+\beta))+C_4)\frac{\dot{A}_1}{r^2} + (B_7(2C_2-C_1(1+\beta))+C_3)\frac{\dot{A}_2}{r^2} + C_1r^\beta\left(\frac{\partial G_{11}}{\partial r}r^{m_1} + G_{11}m_1r^{m_1-1} + \frac{\partial G_{21}}{\partial r}r^{m_2} + G_{21}m_2r^{m_2-1}\right) + 2C_2r^{\beta-1}(G_{11}r^{m_1}+G_{21}r^{m_2}) + (C_1-C_2)b_0r^{b_1+\beta}\sigma_e^{n_0} \tag{43a}$$

$$\dot{\sigma}_\theta = D_1((m_1E_1+2E_2)r^{\beta+m_1-1}) + D_2((m_2E_1+2E_2)r^{\beta+m_2-1}) + (B_8(2E_2-E_1(1+\beta))+E_4)\frac{\dot{A}_1}{r^2} + (B_7(2E_2-E_1(1+\beta))+E_3)\frac{\dot{A}_2}{r^2} + E_1r^\beta\left(\frac{\partial G_{11}}{\partial r}r^{m_1} + G_{11}m_1r^{m_1-1} + \frac{\partial G_{21}}{\partial r}r^{m_2} + G_{21}m_2r^{m_2-1}\right) + 2E_2r^{\beta-1}(G_{11}r^{m_1}+G_{21}r^{m_2}) + (E_1-E_2)b_0r^{b_1+\beta}\sigma_e^{n_0} \tag{43b}$$

$$
\begin{aligned}
\dot{\phi} &= D_1 r^{m_1}\left(L_1+\frac{2L_2}{m_1}\right)+D_2 r^{m_2}\left(L_1+\frac{2L_2}{m_2}\right)-(B_8(2L_2-(1+\beta)L_1)-L_5)\frac{r^{-(\beta+1)}}{(\beta+1)}\dot{A}_1\\
&-(B_7(2L_2-L_1(1+\beta))+L_3)\frac{r^{-(\beta+1)}}{(\beta+1)}\dot{A}_2+\int\left(L_1\left(\frac{\partial G_{11}}{\partial r}r^{m_1}+G_{11}m_1 r^{m_1-1}\right.\right.\\
&\left.\left.+\frac{\partial G_{21}}{\partial r}r^{m_2}+G_{21}m_2 r^{m_2-1}\right)+2L_2(+G_{11}r^{m_1-1}+G_{21}r^{m_2-1})+(L_1-L_2)b_0 r^{b_1}\sigma_e^{n_0}\right)dr+J_1
\end{aligned}
\tag{43c}
$$

$$
\begin{aligned}
\dot{\psi} &= D_1 r^{m_1}\left(P_1+\frac{2P_2}{m_1}\right)+D_2 r^{m_2}\left(P_1+\frac{2P_2}{m_2}\right)-(B_8(2P_2-P_1(1+\beta)L+P_3)\frac{r^{-(\beta+1)}}{(\beta+1)}\dot{A}_1\\
&-(B_7(2P_2-P_1(1+\beta))-P_5)\frac{r^{-(\beta+1)}}{(\beta+1)}\dot{A}_2+\int\left(P_1\left(\frac{\partial G_{11}}{\partial r}r^{m_1}+G_{11}m_1 r^{m_1-1}\right.\right.\\
&\left.\left.+\frac{\partial G_{21}}{\partial r}r^{m_2}+G_{21}m_2 r^{m_2-1}\right)+2P_2(+G_{11}r^{m_1-1}+G_{21}r^{m_2-1})+(P_1-P_2)b_0 r^{b_1}\sigma_e^{n_0}\right)dr+J_2
\end{aligned}
\tag{43d}
$$

The six unknown constants can be achieved using the boundary conditions. The internal and external mechanical pressure and the electric and magnetic potential of the sphere do not vary in time. Thus, we have:

$$
\begin{aligned}
&\dot{\sigma}_r\Big|_{r=a}=0, && \dot{\sigma}_r\Big|_{r=b}=0,\\
&\dot{\phi}_r\Big|_{r=a}=0, && \dot{\phi}_r\Big|_{r=b}=0,\\
&\dot{\psi}_r\Big|_{r=a}=0, && \dot{\psi}_r\Big|_{r=b}=0,
\end{aligned}
\tag{44}
$$

The resultant system of linear equations can be solved in the same as the previous section. To achieve the history of stresses and the electric and magnetic potential through creep progress, the stress rates and the gradient of electric and magnetic potential rate are needed. Firstly, a suitable time increment is selected for timing steps ($dt^{(i)}$). The total time is taken as the sum of timing steps. Thus, for the i[th] time increment, the total time is:

$$
t_i=\sum_{k=0}^{i} dt^{(k)} \tag{45}
$$

For the next timing steps, the radial and circumferential stresses as well as electric and magnetic potential distributions for the previous step are available, and then, the radial and circumferential stress rates are obtained from Eq. (43). Finally, the creep stress and electric and magnetic potential distribution can be found using an iterative method as:

$$
\begin{aligned}
&\Re^{(i)}(r,t_i)=\Re^{(i-1)}(r,t_{i-1})+\dot{\Re}^{(i-1)}(r,t_{i-1})dt^{(i)},\\
&\Re=\sigma_\theta,\sigma_r,\psi,\phi
\end{aligned}
\tag{46}
$$

4. Numerical Results and Discussions

Material coefficients for the FGMEE are used as expressed in Table 1 [12, 25]. The interior and exterior radius of the sphere is considered as $a = 0.1$m and $b = 0.13$m, respectively. The following non-dimensional parameters are used:

$$
\begin{aligned}
&R=\frac{r-a}{b-a},\quad u^*=\frac{u}{a},\quad \sigma_i^*=\frac{\sigma_i}{P_a},\ (i=r,\theta),\\
&\phi^*=\sqrt{\frac{\beta_{11}}{c_{11}}}\frac{\phi}{b},\quad \psi^*=\sqrt{\frac{d_{11}}{c_{11}}}\frac{\psi}{b}\cdot
\end{aligned}
\tag{47}
$$

For the first case, the creep evolution through the time is investigated. The hygro-thermo-magneto-electro-mechanical boundary condition is considered as:

$$
\begin{aligned}
&P_a=10MPa,\quad \phi_a=0,\quad \phi_b=6000,\quad \psi_a=0,\\
&\psi_b=0,\quad T_a=0,\quad T_b=100,\quad M_a=0,\quad M_b=2\cdot
\end{aligned}
\tag{48}
$$

Fig. 2 shows the creep evolution of hollow FGMEE sphere under multiphysical environmental condition and loading. In this analysis, inhomogeneity index β =2 and time increment $dt = 1\times10^5$s is used. As can be seen, radial stress and electric and magnetic potential are time-constant in the inner and outer radii, which satisfies the constant boundary conditions. Regardless of the magnitude, the changes in the rate of stresses, electric and magnetic potentials and displacement, become less significant after 6×10^8s and reaches an approximately steady state after 8×10^8s. According to Figs. 2a, 2e and 2f, the absolute magnitude of radial stress and the electric and magnetic potentials increases with the time at a decreasing rate. From Fig. 2b, it can be observed that the positive hoop stress decreases in time in the inner radius and increases in time in the outer radius. The increases in tensile hoop stress should be considered in design progress as it is the circumferential stress rather than the radial stress which causes failure of the elastic hollow spheres [32, 33].

Fig. 2c shows that the equivalent stress decreases in time in the internal radius, while it exhibits a reverse behavior in the outer radius. Fig. 2d reveals that outward maximum radial displacement is in the inner radii and it decreases smoothly towards the outer radii. Also, the displacement increases at a decreasing rate over time.

In the next case, the effect of inhomogeneity index on the initial and creep behavior of FGMEE thick-walled sphere is revealed. $T_b = 50$ and other boundary conditions are assumed as those of the previous case. Fig. 3 shows the results for different inhomogeneity indexes at initial state of the problem and after 6×10^8s.

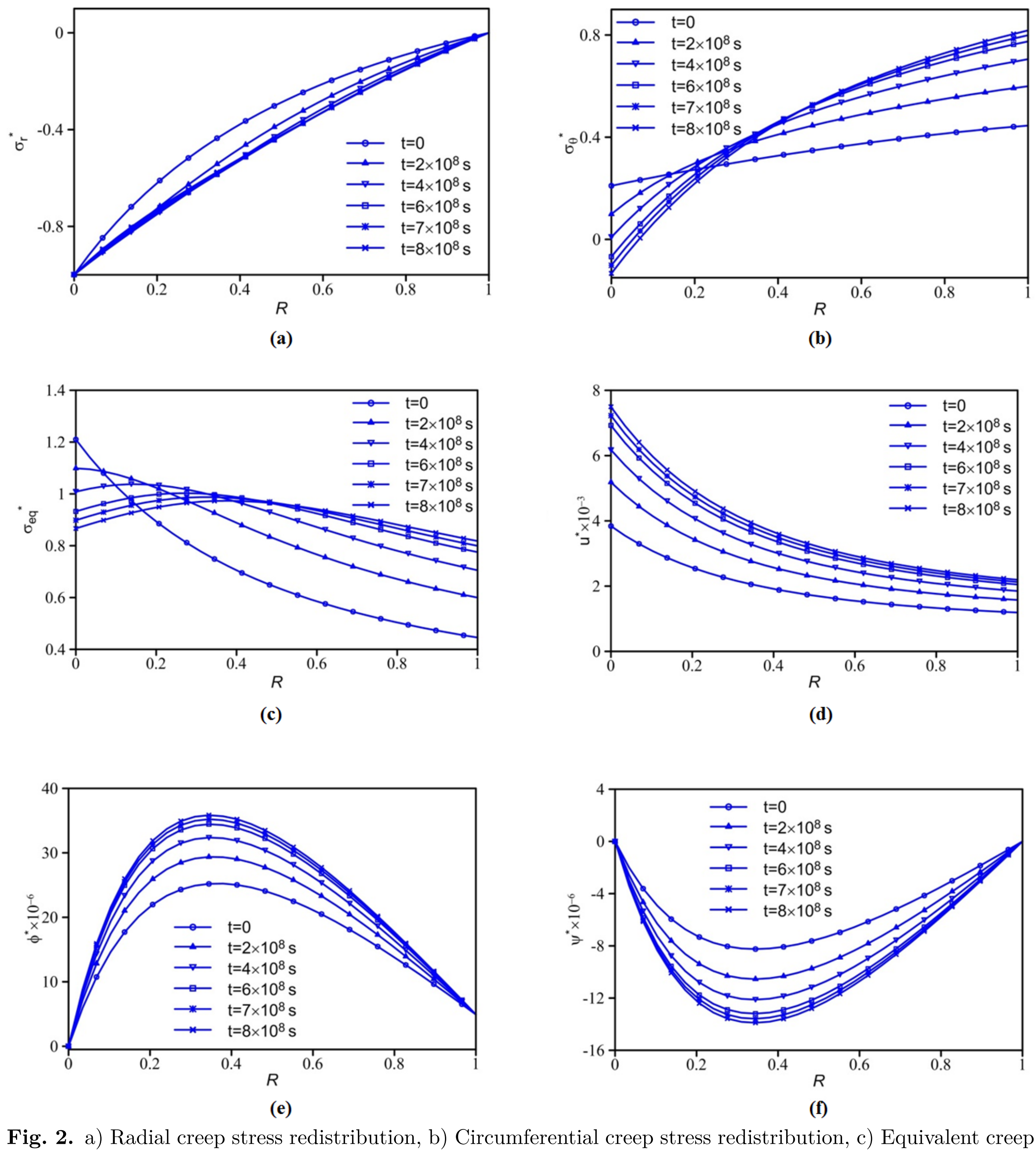

Fig. 2. a) Radial creep stress redistribution, b) Circumferential creep stress redistribution, c) Equivalent creep stress redistribution, d) Radial displacement histories, e) Electric potential and f) Magnetic potential histories during creep evolution.

Table 1
Material constants.

c_{11}(GPa)	c_{12}(GPa)	c_{23}(GPa)	c_{22}(GPa)	e_{11}(C/m^2)
215	120	120	218	7.5
e_{12}(C/m^2)	α_r(1/K)	α_θ(1/K)	q_{11}(N/Am)	q_{12}(N/Am)
-2.5	6×10^{-6}	15×10^{-6}	345	265
β_{11}(C^2/Nm^2)	d_{11}(Ns^2/C^2)	ε_{11}(Ns/VC)	β_2(m^3/kg)	β_θ(m^3/kg)
5.8×10^{-9}	95×10^{-6}	2.82×10^{-9}	0.8×10^{-4}	1.2×10^{-4}
m_1(N/AmK)	χ_1(Cm/kg)	P_1(C^2/m^{2}k)	γ_1(Nm^2/Akg)	n_0
2.5×10^{-5}	0	-2.5×10^{-5}	0	3
b_1	b_0	ρ		
-5	0.11×10^{-36}	7750		

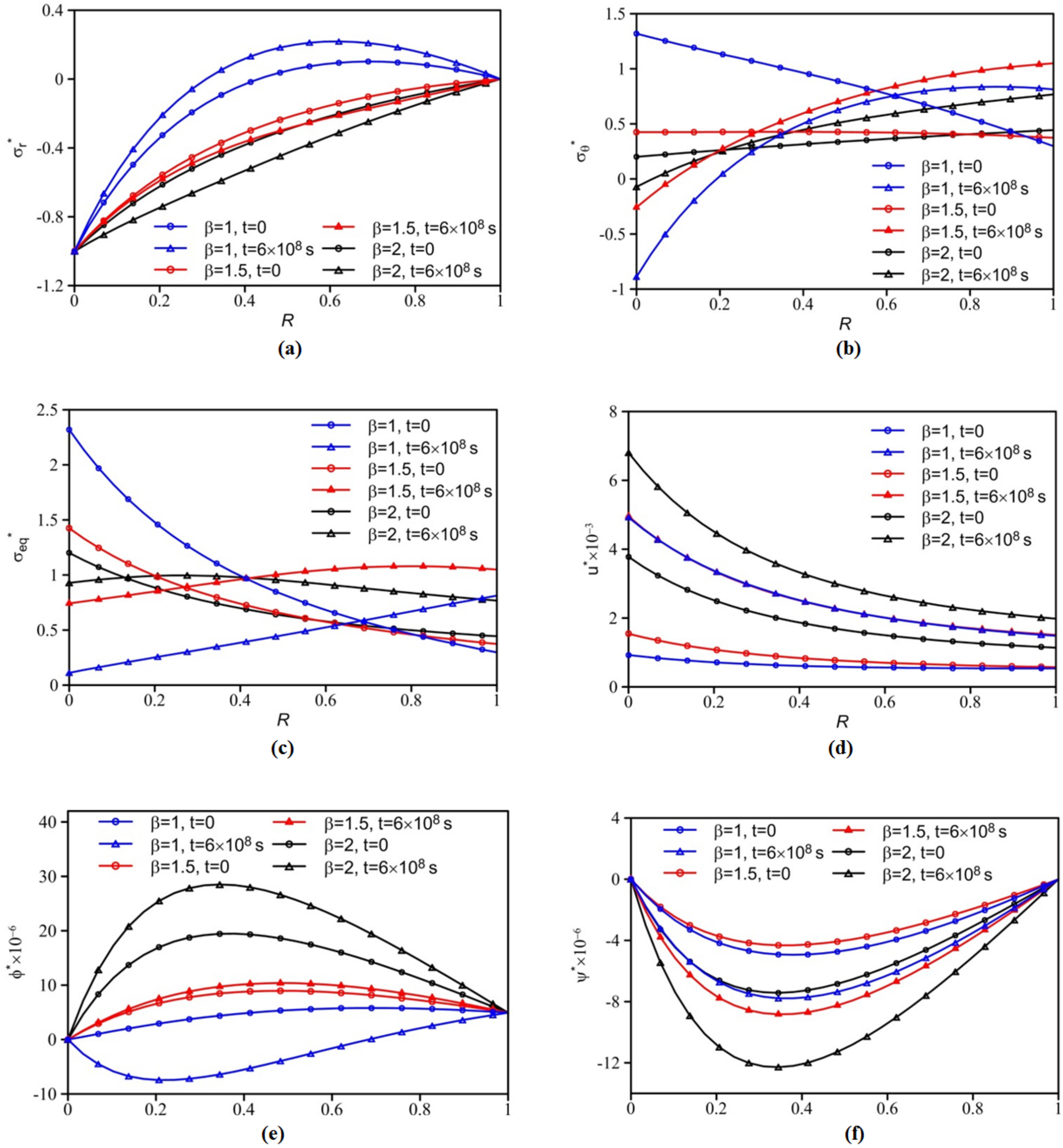

Fig. 3. Effect of inhomogeneity index on the a) Radial stress, b) Circumferential stress, c) Equivalent stress, d) Radial displacement (e) Electric potential and f) Magnetic potential.

According to Fig. 3a, increases in β results in increases in both the initial and creep radial stresses at a decreasing rate. However, the magnitude of the the increase is more significant after creep occurs. Therefore, the magnitude of β has more effects on the behavior of the structure after creep occurs. In the case $\beta = 1$, the radial stress becomes tensile in some radii due to the fact that creep progresses after 6×10^8s. Therefore, the proper value of β must be considered for the FGMEE in modern technologies because these ceramics are mechanically brittle and are very sensitive to tensile loads and may not be usable after some years. Fig. 3b shows that changes in hoop stress are more significant for a smaller value of β, especially near the interior surface. This is also correct for equivalent stress in Fig. 3c. Fig. 3d shows that the radial displacement after creep progress is less affected by the value of β. As shown in Fig. 3e, the effect of different values of β on the electric potential distribution is more significant after creep occurs. Moreover, changes in the value of β results in changes in the curvature direction as well as the sign of electric potential. Fig. 3f shows the effect of β on the magnetic potential distribution through the radius of the sphere both before and after creep occurs. It is worth mentioning that the equations are nonlinear functions of grading index. Consequently, the FGMEE exhibits no even alterations due to changing the grading index.

The effect of hygrothermal loading on the primitive and creep response of the FGMEE sphere is considered for the next case. The moisture concentration and temperature on the interior radii are considered to be zero, while the moisture concentration and temperature increase on the exterior surface. In this case, $\beta = 1.5$ and $M_b = T_b/200$ are assumed and other boundary conditions are as those of the previous one. The results are shown in the Fig. 4.

According to Fig. 4a, increases in hygrothermal loading on the outer surface results in decreases in compressive radial stress both for initial and creep cases. The radial stress becomes positive for more rises in the hygrothermal loading. Besides, changes in creep radial stress caused by rising hygrothermal loading is more significant in comparison to primitive radial stress. Consequently, the effect of hygrothermal loading after creep progress is more important rather than static problem. Regarding Fig. 4b, both initial and creep circumferential stress are increased by rising the hygrothermal loading. Also, there is a fix point near the inner radius for primitive hoop stress and near the outer radius for creep hoop stress so that the hoop stress is independent of hygrothermal loading.

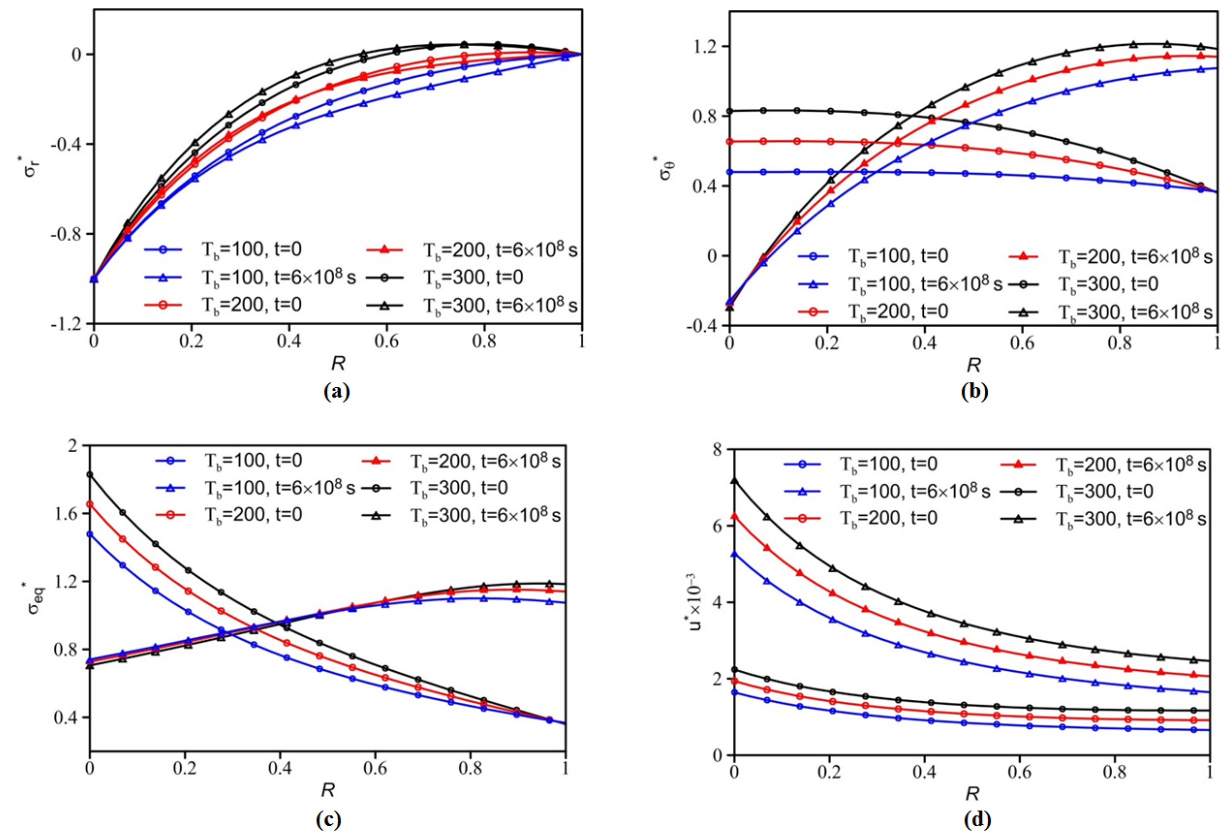

Fig. 4. Effect of hygrothermal loading on the a) Radial stress, b) Circumferential stress, c) Equivalent stress, d) Radial displacement.

In addition, the maximum circumferential stress for the initial state is located near the inner surface. Conversely, the maximum circumferential stress is located near the outer surface after creep progress. Fig. 4c depicts that the equivalent stress is maximum near the inner radius for the static case, while it is vice versa after creep progresses. As demonstrated in Fig. 4d, an increase in applied hygrothermal loading leads to rises in both primitive and creep outward radial displacement.

To disclose the influence of temperature and moisture dependence of the elastic coefficients on the static response, the elastic coefficients can be expressed in the following form [17]:

$$C_{ij} = C_{ij0}(1 + \alpha^* T + \beta^* M) \tag{49}$$

in which C_{ij0} is the temperature and moisture independent elastic coefficient, α^* and β^* are empirical material coefficients for the temperature and humidity dependence. In this research, the temperature and humidity dependence is only assumed for even temperature and moisture concentration increases so as to have no non-linear equations. In this case, the sphere is under uniform temperature and moisture concentration increases, $T = 100$, $M = 5$ and we have: $Pa = 1\text{MPa}$, $\beta = 1.5$. Other boundary conditions are kept unchanged. Figs. 5 and 6 illustrate the influence of the temperature and humidity dependence of the elastic coefficients on the primitive and creep response of the FGMEE sphere, respectively. Due to similarity of the influence of the temperature and moisture concentration on the multiphysical response, the same magnitudes are used for the empirical constants of temperature and humidity dependence, while $\alpha^* = \beta^* = 0$ indicates the material properties which are independent of temperature and humidity.

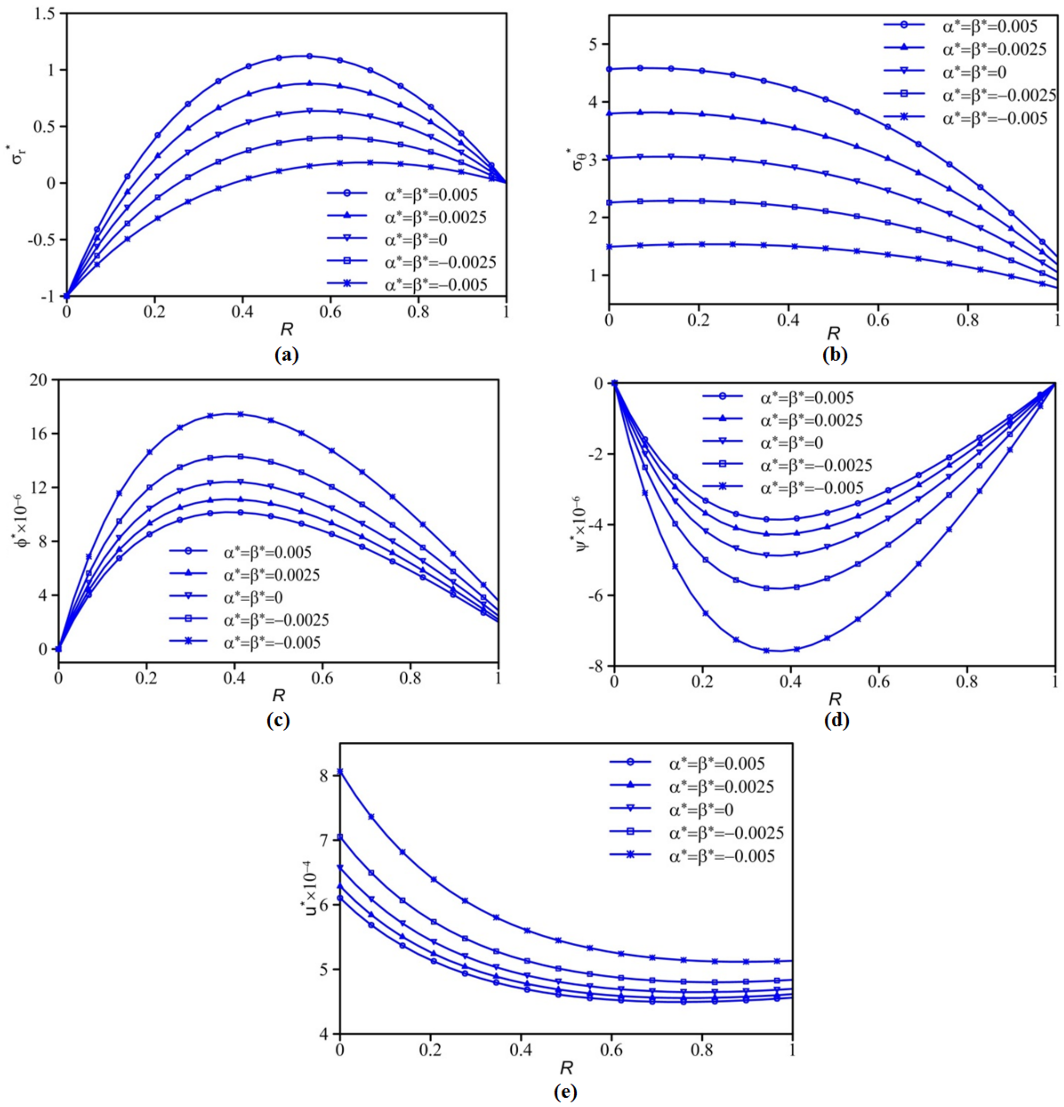

Fig. 5. Effect of temperature and moisture dependency of the material coefficients on the distribution of initial elastic a) Radial stress, b) Circumferential stress, c) Electric potential, d) Magnetic potential and e) Radial displacement.

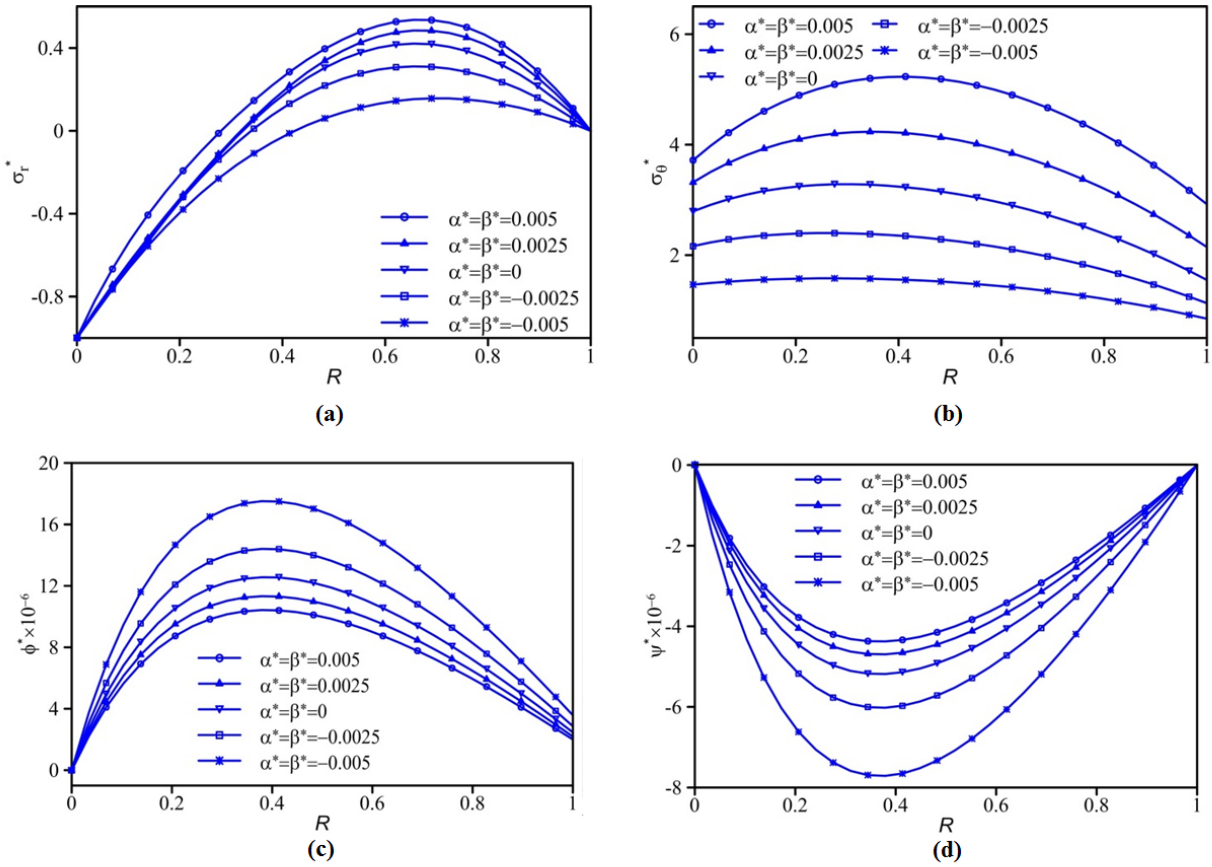

Fig. 6. Effect of temperature and moisture dependency of the elastic coefficients on the distribution of final creep a) Radial stress, b) Circumferential stress, c) Electric potential and d) Magnetic potential.

According to Figs. 5a and 6a, positive value of empirical constants increases the tensile radial stress, whereas the negative magnitude has a reverse influence. The effect of temperature and humidity dependency on the primitive radial stress is more significant in comparison with creep radial stress. Figs. 5b and 6b show the circumferential stress increases for positive value of empirical constants while the effect of minus value is vice versa. The changes are more intensive near the inner radius for initial stress. Figs. 5c and 5d as well as Figs. 6c and 6d depict that positive value of empirical constants leads to a decrease in electric and magnetic potential of each point while the negative one has a reverse effect. Fig. 5e illustrate that positive value of empirical constants reduces the outward radial displacement, and reversely, the minus value of empirical constants enhances the radial displacement.

To the best of author's knowledge, there is no available paper in the literature for time-dependent creep analysis of MEE spheres. However, static behavior of FGMEE spheres has been studied in Ref. [12]. Thus, to verify the results, the radial and hoop stress distributions is compared in Fig. 7. The details of non-dimensional parameters and material constants can be found in Ref. [12]. In this case: Pa=2KPa, Tb=2, Φ_b=2000 and other boundary conditions are kept at zero. As can be seen, the present results have a very good agreement with reported in Ref. [12].

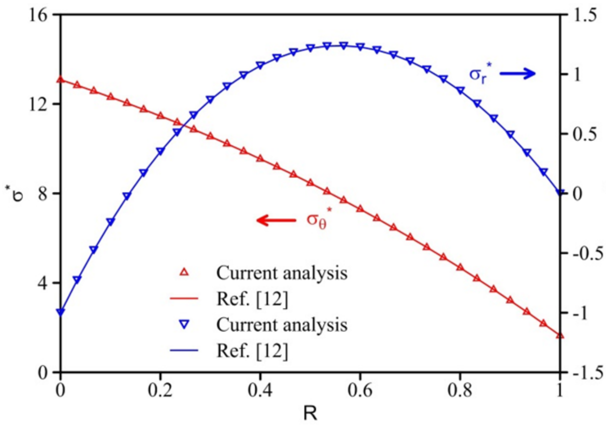

Fig. 7. Radial and circumferential stresses.

5. Conclusions

The time-dependent creep analysis is carried out for a functionally graded magneto-electro-elastic thick-walled sphere under an axisymmetric hygro-thermo-magneto-electro-mechanical loading. The solution is achieved by using the Prandtl-Reuss equations and Norton's law. The conclusions can be as following:

- Regardless of the magnitude, the changes in the rate of stresses, electric and magnetic potentials and displacement, become less significant after 6×10^8s and reaches an approximately steady state after 8×10^8s.

- The absolute value of radial stress, radial displacement as well as electric and magnetic potentials is increasing in time at a decreasing rate. Also, the positive hoop stress decreases in time at the inner radius and increases in time at the outer radius with decrease rates

- Increases in inhomogeneity-index leads to more increases in the creep radial stress rather than primitive radial stress. The effect of different value of on the electric potential distribution is more significant after creep occurs.

- Changes in creep radial stress caused by rising hygrothermal loading is more significant in comparison to primitive radial stress. Consequently, the effect of hygrothermal loading after creep progress is more important than static problem. Initial and creep circumferential stress and radial displacement increase as a result of rising the hygrothermal loading.

- Positive value of empirical constants increases the radial and circumferential stresses in both initial and creep state. Also, it decreases electric and magnetic potentials, while the minus value has a reverse effect. The effect of temperature and moisture dependency on the primitive radial stress is more significant in comparison with creep radial stress.

References

[1] H.S. Tzou, H.J. Lee, S.M. Arnold, Smart materials, precision sensors/actuators, smart structures, and structronic systems, Mech. Adv. Mater. Struct., 11(4-5) (2004) 367-393.

[2] N. Habibi, S. Asadi, R. Moradikhah, Evaluation of SIF in FGM thick-walled cylindrical vessel, J. Stress Anal., 2(1) (2017) 57-68.

[3] M. Omidi bidgoli, A. Loghman, M. Arefi, The effect of grading index on two-dimensional stress and strain distribution of fg rotating cylinder resting on a friction bed under thermomechanical loading, J. Stress Anal., 3(2) (2019) 75-82.

[4] M. Saadatfar, M. Aghaie-Khafri, Electromagnetothermoelastic behavior of a rotating imperfect hybrid functionally graded hollow cylinder resting on an elastic foundation, Smart Struct. Syst., 15(6) (2015) 1411-1437.

[5] M. Saadatfar, M. Aghaie-Khafri, On the magneto-thermo-elastic behavior of a FGM cylindrical shell with pyroelectric layers featuring interlaminar bonding imperfections rested in an elastic foundation, J. Solid Mech., 7(3) (2015) 344-363.

[6] M. Saadatfar, M. Aghaie-Khafri, Thermoelastic analysis of a rotating functionally graded cylindrical shell with functionally graded sensor and actuator layers on an elastic foundation placed in a constant magnetic field, J. Intel. Mater. Sys. Struct., 27(4) (2015) 512-527.

[7] H.L. Dai, H.J. Jiang, L. Yang, Time-dependent behaviors of a FGPM hollow sphere under the coupling of multi-fields, Solid State Sci., 14(5) (2012) 587-597.

[8] H.M. Wang, H.J. Ding, Transient responses of a magneto-electro-elastic hollow sphere for fully coupled spherically symmetric problem, Eur. J. Mech. A Solids, 25(6) (2006) 965-980.

[9] H.M. Wang, H.J. Ding, Radial vibration of piezoelectric/magnetostrictive composite hollow sphere, J. Sound Vib., 307(1-2) (2004) 330-348.

[10] Y. Ootao, M. Ishihara, Exact solution of transient thermal stress problem of a multilayered magneto-electro-thermoelastic hollow sphere, Appl. Math. Model., 36(4) (2012) 1431-1443.

[11] J.Y. Chen, E. Pan, P.R. Heyliger, Static deformation of a spherically anisotropic and multilayered magneto-electro-elastic hollow sphere, Int. J. Solids Struct., 60(60-61) (2015) 66-74.

[12] M. Saadatfar, M. Aghaie-Khafri, Hygrothermomagnetoelectroelastic analysis of a functionally graded magnetoelectroelastic hollow sphere resting on an elastic foundation, Smart Mater. Struct., 23(3) (2014) 035004.

[13] W. Smittakorn, P.R. Heyliger, A discrete-layer model of laminated hygrothermopiezoelectric plates, Mech. Compos. Mater. Struct., 7(1) (2000) 79-104.

[14] W. Smittakorn, P.R. Heyliger, An adaptive wood composite: theory, Wood Fiber Sci., 33(4) (2001) 595-608.

[15] S. Raja, P.K. Sinha, G. Prathap, D. Dwarakanthan, Thermally induced vibration control of composite plates and shells with piezoelectric active damping, Smart Mater. Struct., 13(4) (2004) 939-950.

[16] M. Saadatfar, M. Aghaie-Khafri, On the behavior of a rotating functionally graded hybrid cylindrical shell with imperfect bonding subjected to hygrothermal condition, J. Therm. Stresses, 38(8) (2015) 854-881.

[17] M. Saadatfar, M. Aghaie-Khafri, Hygrothermal analysis of a rotating smart exponentially graded cylindrical shell with imperfect bonding supported by an elastic foundation, Aerosol Sci. Technol., 43 (2015) 37-50.

[18] M. Saadatfar, Effect of multiphysics conditions on the behavior of an exponentially graded smart cylindrical shell with imperfect bonding, Meccanica, 50(8) (2015) 2135-2152.

[19] L.H. You, H. Ou, Steady-state creep analysis of thick-walled spherical pressure vessels with varying creep properties, J. Pressure Vessel Technol., 130(1) (2008) 014501-1-014501-5.

[20] A. Loghman, N. Shokouhi, Creep damage evaluation of thick-walled spheres using a long-term creep constitutive model, J. Mech. Sci. Technol., 23 (2009) 2577-2582.

[21] A. Loghman, A. Ghorbanpour Arani, S.M.A. Aleayoub, Time-dependent creep stress redistribution analysis of thick-walled functionally graded spheres, Mech. Time-Depend Mater. 15(4) (2011) 353-365.

[22] A. Loghman, S.M.A. Aleayoub, M. Hasani Sadi, Time-dependent magnetothermoelastic creep modeling of FGM spheres using method of successive elastic solution, Appl. Math. Model., 36(2) (2012) 836-845.

[23] J. Jafari Fesharaki, A. Loghman, M. Yazdipoor, S. Golabi, Semi-analytical solution of time-dependent thermomechanical creep behavior of FGM hollow spheres, Mech. Time-Depend Mater., 18(1) (2014) 41-53.

[24] A. Ghorbanpour Arani, R. Kolahchi, A.A. Mosallaie Barzoki, A. Loghman, The effect of time-dependent creep on electro-thermo-mechanical behaviors of piezoelectric sphere using Mendelson's method, Europ. J. Mech. A Solids, 37 (2013) 318-328.

[25] M. Jabbari, M.S. Tayebi, Time-dependent electro-magneto-thermoelastic stresses of a poro-piezo-functionally graded material hollow sphere, J. Pressure Vessel Technol., 138(5) (2016) 051201-1-051201-12.

[26] A. Loghman, H. Tourang, Non-stationary electro-thermo-mechanical creep response and smart deformation control of thick-walled sphere made of polyvinylidene fluoride, J. Braz. Soc. Mech. Sci. Eng., 38(8) (2016) 2547-2561.

[27] M. Saadatfar, Effect of Interlaminar Weak bonding and constant magnetic field on the hygrothermal stresses of a FG hybrid cylindrical shell using DQM, J. Stress Anal., 3(1) (2018) 93-110.

[28] M.R. Eslami, M.H. Babaei, R. Poultangari, Thermal and mechanical stresses in a functionally graded thick sphere, Int. J. Press. Vessels Pip., 82(7) (2005) 522-527.

[29] M. Saadatfar, Time-dependent creep response of magneto-electro-elastic rotating disc in thermal and humid environmental condition, AUT J. Mech. Eng., (In Press), DOI: 10.22060/AJME.2019.15375.5770.

[30] M. Saadatfar, Analytical solution for the creep problem of a rotating functionally graded magneto-electro-elastic hollow cylinder in thermal environment, Int. J. Appl. Mech., (In Press), DOI: 101142/S1758825119500534.

[31] M. Saadatfar, Stress redistribution analysis of piezomagnetic rotating thick-walled cylinder with temperature-and moisture-dependent material properties, J. Appl. Comput. Mech., 6(1) (2020) 90-104.

[32] A. Ghorbanpour, S. Golabi, M. Saadatfar, Stress and electric potential fields in piezoelectric smart spheres, J. Mech. Sci. Technol., 20(11) (2006) 1920-1933.

[33] M. Saadatfar, A. Rastgoo, Stress in piezoelectric hollow sphere with thermal gradient, J. Mech. Sci. Technol., 22 (2008) 1460-1467.